FOURTH EUROPEAN ROTORCRAFT
AND POWERED LIFT AIRCRAFT FORUM

PAPER Nº 10

2D SIMULATION OF UNSTEADY PHENOMENA ON A ROTOR

by

J - Renaud Snias

J - Coulomb Ceat

AEROSPATIALE, HELICOPTER DIVISION,
MARIGNANE, FRANCE

September 13-15 1978
STRESA ITALY

ASSOCIAZIONE ITALIANA DI AERONAUTICA ED ASTRONAUTICA
ASSOCIAZIONE INDUSTRIE AEROSPAZIALI

1. UNSTEADY AERODYNAMICS : ONE OF THE KEY FACTORS ON A ROTOR ?

The intense commercial competition facing the Aeronautical World is only a reflection of the problems and needs of the present period. It imposes large industrial mutations and guides the technological choices. The rotorcraft industry does not escape to this general trend, where the key words are :

- Performance increase. Energy saving.
  Operating envelope (both civil and military) wider in a very diversified environment. Operating costs reduced. Greater operating safety. Better «man/machine» interface.

Such are the present great trends in the helicopter world (Ref 1)
They impose :

- good calculation and experimental methods to solve technical problems.
- a fundamental knowledge of basic phenomena governing helicopter operation.

As regard rotors, the diversity and complexity of prediction methods are at the measure of the physical phenomena involved in rotary wing operation and limit their use (reference 2). With these methods, particularly for the aerodynamic aspects, it is possible to have a thorough knowledge of rotors (reference 3) and set-back the operating limits of the conventional helicopter (reference 4).

It is a passionating and often mysterious field of investigation !

From the large amount of studies conducted in the last ten years, we shall retain, for our purpose, this noteworthy fact :
«In the calculation of rotors, nobody cannot ignore any longer the unsteady effects».

The comparison between theoretical calculations and flight or wind tunnel test results, the determination of loads and performance (references 5 through 8), the solution of dynamic problems (references 9 through 13), the development of new formula (reference 14) demonstrate how the notions of steady aerodynamics are insufficient and sometimes not acceptable.

Unfortunately, rotor aerodynamics present a great complexity due to its powerful coupling with the rotor blade and head aeroelasticity factors (references 15 and 16) and also because it is dependent on many interacting and hardly dissociable parameters (reference 17) : unsteady flow, 3-D effects, compressibility, induced velocity field.....

This explains the difficulty of isolating each aerodynamic parameter to know its influence and define its significance, this being required to define rotor models allying simplicity and accuracy.

2. ROTOR UNSTEADY AERODYNAMICS : The various approaches.

The combination of rotation and forward motions, pitch cyclic control, flapping and drag motions together with blade elastic deformations, results in a periodic modulation, both in amplitude and direction, of the attack velocities on every blade section. To this modulation are superimposed fluctuations due to blade interactions with each other and various disturbances. Therefore, the helicopter rotor is a very unsteady device, due on the one hand, to the motion of lifting bodies (blades) and, on the other hand, to the variations in velocity of the fluid surrounding these bodies (Figure 1).

With the passage from the «ring» type methods, based on momentum considerations (reference 18) to models taking into account each blade and its wake (reference 18), it has been possible to take into account progressively part of these unsteady phenomena.

Thus, usual methods are generally linear methods dealing with perfect fluids and calling on lifting lines or surfaces with rigid wake while associating simplified limit conditions (small disturbances) with the solution of Laplace's equation or wave equation for the velocity potential (Reference 20). In reality, these methods are accurate for medium tip speed ratios only. They lose their accuracy for hover or low speed conditions (particularly if the rotor is highly loaded), for which the unsteady distribution of loads is strongly affected by the near wake. (Reference 21). Therefore, wake distortions, due to self-induction or mutual interactions of the various vortex-generating components, impose for calculations, either the equilibrium of wakes or, in a simpler manner, the use of more realistic «prescribed wakes» (Reference 22)

Further, these methods loose, their efficiency for high speeds and/or highly loaded rotors, due to significant non-linearities appearing both on the advancing blade (transsonic disturbances) and retreating blade (dynamic stall).

With the modern digital methods it is possible, for supercritical flows, to deal with cases of increasing complexity (Reference 23). On the contrary, it sums that the processing of retreating blade non-linearities should, to be efficient, call on experimental or semi-empirical elements obtained by two-dimensional simulationn of the retreating blade dynamic stall in the form of corrections made to the linear concept (Reference 24).

3. THE TWO-DIMENSIONAL SIMULATION : A tool or a trap for the designer ?

In splite of the progress made in the study of laminar, or even turbulent, boundary layers (Reference 25) these methods are still of a too fundamental nature to be used directly by the designer.

Therefore, the two-dimensional simulation will be a powerful tool allowing the experimental determination of aerodynamic unsteady factors, which cannot be calculated.

Usually, rigs with harmonic oscillation are used, this simplifying the experimental procedures and offering a practical interest when the rotor model solves, the rotor response equations through a linear system calling on a harmonic break-down of the azimuthal variation (Ref. 20)

Further, modern airfoils are defined at present using steady methods (References 26 and 27). Therefore, experimental the results obtained on harmonic oscillation rigs provide valuable data on aerodynamic and the dynamic behaviour of airfoils used on rotor blades. However, the results, obtained in this manner, must be processed prudently. Emphasis should be placed on the fact that by studying elementary harmonic motions, such as oscillations in pitch (References 28 through 30), plunging (References 28 and 29 , and lead-lag motions (References 31 and 32), it is attempled to solve a highly non linear problem (dynamic stall) according to a linear concept. At last, it is to be pointed out that indicial type motions may be better adapted to the reality of some rotor configurations (Vortex type interactions) and to some mathematical solution procedures (step-by-step solution in azimuth) (Reference 33).

4. CONDITIONS OF TWO-DIMENSIONAL SIMULATION

If the linear principle of superimposition effect for the various motions is admitted, and if the radial flows occuring on a blade are neglected, 2D-unsteady simulation may be made for every motion corresponding to the various blade degrees of freedom.

In this paper, we shall discuss the pitch harmonic oscillations only.

The various similitude parameters to be observed are :

4.1 OF A GEOMETRICAL OR DYNAMIC NATURE:

- airfoil geometry
- mean angle of attack α_m and pitch oscillation amplitude $\bar{\alpha}$ values. Which should correspond to the usual values of collective and cyclic pitches as well as to blade responses to the airloads.
- reduced oscillation frequency as the time derivatives of the airfoil angle of attack are proportional to the frequency and as, in the linear theory, aerodynamic coefficients are depending on these time derivatives and furthermore as the action of unsteady wakes on the chordwise pressure distribution is expressed also, more or less esplicitely, in terms of the reduced frequency (for instance, Theodorsen's function) (Reference 34).

The envelope of mean angle of attack variations should exceed the airfoil steady stall angle.

Amplitude and reduced frequency are linked by the type of simulation to be made. If the blade forced response problem is studied, large amplitudes (cyclic pitch) will have to be used at reduced frequencies corresponding to the rotor fundamental frequency (1 Ω). Then, the reduced frequency is linked to the Mach number (figure 2). On the contrary, to deal with dynamic problems linked to the blade stability under torsion loads, low amplitudes will be used but at higher frequencies, ranged up to the level corresponding to first torsional mode of rotor blades (ω_θ).

4.2 LINKED TO COMPRESSIBILITY

The Mach numbers met on the retreating blade is to be simulated.

4.3 LINKED TO VISCOSITY

- Reynolds number related to the chord.
- Position of forced or natural boundary layer transition.

5. THE C.E.A.T. OSCILLATION TEST SET-UP

Result of the experience acquired over several years, this set-up meets the similitude requirements stated above (Reference 35).

5.1 THE C.E.A.T. «S-10» WIND-TUNNEL

The tests have been conducted in the S-10 subsonic wind-tunnel of the C.E.A.T. in Toulouse. This wind-tunnel, in which the stagnation pressure is equal to atmospheric pressure, gives a maximum speed of 140 m/sec. and has a rectangular test section (2.2 m x 1 m) (figure 3).

The various experimental campaigns have been run at M = 0.12 – 0.2 – 0.3 et 0.4, this corresponding to representative Reynolds numbers ranging from 1.1×10^6 to 3.9×10^6 for a 0.4 m. chord.

5.2 OSCILLATING TEST RIG

The original test rig developed has better performance than conventional systems. Its interest lies in the production of a harmonic motion with a negligible distortion rate, taking into account the large loads applied to the wing and due to :

- inertia loads at high oscillation frequencies
- aerodynamic loads giving very large pitching moment variations around the stalling angles of attack, specially for large amplitudes.

The essential part of the rig (figure 4) is a mechanical unit, pressure lubricated, placed on one side of the wing and secured on the wind-tunnel wall outside the test section. It converts the uniform rotating motion of a hydraulic motor vertical shaft (maximum power : 8 kw) into an oscillating angular motion of a horizontal shaft.

This output shaft is extended by a cone having two functions :

- its base, flush with the test section wall, constitutes a protection plate for the airfoil ; a P.T.F.E. seal is provided between the fixed wall and the cone base to present leakage.
- it ensures the mechanical link with the wing.

Oscillation amplitude, adjustable from 0 to ± 6°, is measured by two sensors located on the oscillation axis on either side of the wing. Due to the models used, permissible amplitudes are :

$\bar{\alpha} = \pm 6^{\circ}$ at $f = 8$ Hz and $\bar{\alpha} = \pm 1^{\circ}$ at $f = 40$ Hz

The complete mechanical unit can rotate inside a fixed framework. With this rotation, it is possible to set the airfoil mean angle of attack α_m through a remote control arm actuated by the wind-tunnel scale.

At last, motion governing is made throug a tachometer generator, located on the driving shaft, and its signal controls the hydraulic motor servo-valve, which has a high bandwidth (100 Hz) and is located against the motor to ensure the best possible response time of the governing system.

5.3 AIRFOIL MODELS

Models are two-dimensional wings, having a span of 1 metric and a chord of 0.4 metric, placed horizontally in the centre of the test section, between the side walls of the wind tunnel. They are installed without protection plate and a 2 mm. clearance at their sides allow their oscillations without contact with the walls.

These wings must have a maximum torsional rigidity. They are filled with polymethane foam, a light material with reduced inertia. The structure consists of a metal framework, ensuring flexural rigidity, and includes a fluid bearing supporting a fixed shaft (located at 25 % of chord) secured to the test section walls and around which the model oscillates. The wing is covered by a resin impregnated glass fibre skin ensuring torsional rigidity and produced in a mould made to final dimensions.

5.4 INSTRUMENTATION AND DATA SYSTEM

Miniature differential pressure tranducers are used. They are located within the wing so that their sensitive diaphragm is parallel to the oscillation direction, thus they are not affected by accelerations. Each tranducer is located near two pressure ports to which it is connected. The wings produced to date are provided with 13 tranducers measuring the differential pressure between the upper and lower surfaces at the same chordwice position along a cross-section corresponding nearly to the nuid wing section. The pipe length between the pressure ports and tranducers limits the bandwidth of measures, but checks have shown that it remains greater than 200 Hz on all the transducers, which is sufficient for our purpose.

Figure 5 shows details of transducer installation. Each transducer box is imbedded in a flexible elastomer to prevent wing stresses interactions.

The pressure sensor signals are transmitted to a 14-track magnetic recorder, then processe, using the Fourier's analysis method, over several successive periods as regard the oscillation frequency and its various harmonies. The processed results are then filtered and the continuous term and the first three harmonies only are retained. With this procedure, the non-repeatability of phenomena is not a problem, while sufficiently accurate and consistent results are obtained if only global aerodynamic coefficients are considered.

Figure 6 shows an example of pressure measurement and the result obtained by this data processing method and the result.

These pressure measurements are supplemented by the use of hot films which, it is well known (reference 36). Constitute a powerful tool for the qualitative study of boundary layer local behaviour. These hot films, placed perpendicular to the flow, are bonded on the model upper surface together with their associated resistances closing the electric bridge (figure 7). Having a bandwidth exceeding 1000 Hz, they are very sensities to the condition of the surrounding boundary layer. The transition angle of attack α_T may be detected without any ambiguity (figure 7 - upper curve) as it corresponds to a significant increase in the mean signal level.

These hot films are also very sensitive to local speed fluctuations, they allow the determination of areas where large variations exist such as vortex phenomena, bubble or full stall (figure 7, lower curve).

The angle of attack α_{BF} which corresponds to the beginning of the fluctuations is, generally close to stall.

This last phenomena not being strictly periodic, a better representation is obtained by computer processing of the signals accended on photographic paper, and magnetic tape. Further, the time average and standard deviation, calculated from 100 points of about 15 successive periods, are determined. Thus, the characteristic angle of attack α_T and α_{BF} are defined from the «standard deviation VS. angle of attack» curve.

6. ANALYSIS OF GLOBAL UNSTEADY RESULTS

6.1 PRACTICAL EFFECTS OF DYNAMIC STALL

The tests on oscillating models are essentially related to what, by convertion, is called «dynamic stall». We will come back later on the physical phenomena covered by this term and on the attempts made to explain them We shall take the dynamic stall definition from reference (37) :

«A set of aerodynamic phenomena occurring when an airfoil is submitted to aerodynamic conditions variable in time, and resulting in lift loss or sudden increase in pitching moments which characterize stall configurations»

The dynamic effects being quantified with respect to the airfoil steady aerodynamic characteristics, the angle of attack is an input value generally used.

Figure 8 summarizes the conventional influence of the unsteady flow for various values of the mean angle of attack α_m for the SA 13109-1.58 airfoil, all other parameters being fixed.

It is noted :

- the existence of lift and moment hysteresis loops, small or negligible at mean angle of attack smaller than the steady stall angle and at low frequency but becoming really significant when α_m is close to this angle or greater.
- Maximum lift values greater than the steady value, mainly at oscillations close to the steady stall angle. This increase in CN max reflects quantitatively the beneficial influence of the unsteady effects and stall delay.
- The appearance of a moment stall before lift stall.
- The existence of maximum nose-down moments (C_M max.) which, at high mean angle of attack, are greater than the steady moments and reflect quantitatively the prejudiciable effect of the dynamic stall on blades.
- At last, the appearance of a rigidity and, particularly, of an aerodynamic damping due to the fact that the moment and motion are out-of-phase.

The algebraical area of the moment loops is proportional to the net work of aerodynamic forces during a cycle, and thus it is possible to quantify the aerodynamic damping. Under some conditions, the moment cycle is running clockwise. The work of aerodynamic forces is then positive, this corresponding to a negative aerodynamic damping and may have prejudiciable effects on the blade torsional stability.

Thus, the maximum normal lift C_N max, the maximum nose down moment C_M max. and the reduced aerodynamic damping S* are the three global values, having a practical interest for the designer.

Therefore, let us review briefly the effect of the various parameters on these values.

6.2 EFFECT OF AIRFOIL SHAPE

As in steady aerodynamics, the airfoil shape has obviously a great influence on aerodynamic characteristics. As a rule, when several airfoils are compared , their «unsteady flow» classification is identical with that in «steady flow»

On figure 9, the «thickness law» effect may be noted for two airfoils having the same mean-line and the same leading edge radius. Thinning-down lowers the C_N max. level and advances the appearance of large C_M max. When angle of attack increases. «Instability pockets» appear also somer. Figure 10 shows the beneficial effect of thickness and camber on the angle of attack at the beginning of instability.

6.3 EFFECT OF COMPRESSIBILITY

The wind tunnel maximum flow velocity ($M = 0.4$) does not allow the appearance of transsonic troubles on the airfoil upper surface. However, it is sufficient to achieve supercritical configurations.

Figure 11 shows. at reduced iso-frequency, that compressibility lowers the angle of attack at the beginning of instability and limits the C_N max level achieved. This phenomenon would be still more pronounced at iso-frequency.

6.4 EFFECT OF REDUCED FREQUENCY

The single parameter representing the unsteady flow in linear conditions, the reduced frequency, is also a fundamental parameter in non-linear conditions. In fact, stall delay depends directly on the reduced frequency. Thus, figure 12 shows that it is possible to achieve C_N max values all the more greater than the frequency is higher (For the OA 209 airfoil, the maximum normal lift value is 1.28 in steady conditions at $M = 0.12$). The increase in frequency delays also the beginning of instability. However, the aerodynamic damping and moment values depend on the shape of the hysteresis loops. Then, the other parameters (α_m and $\bar{\alpha}$) are to be considered, the dynamic stall phenomena being different if they are occurring with increasing or decreasing angle of attack.

6.5 EFFECT OF OSCILLATION AMPLITUDE

In the linear theory, the aerodynamic loads are proportional to the amplitude (reference 34). This explains why, at moduate reduced frequencies corresponding to small out-of-phase values, only one linear curve reflects the variation of C_N max versus α max. (figure 13). In dynamic stall conditions, highly non-linear, the effect of amplitude becomes significant. At iso-α max (same type of stall), it is possible to achieve higher C_N max by an increase in amplitude. This is due to the fact that the angular velocity $\dot{\alpha}$ is proportional to $\bar{\alpha}$. The beneficial effect of an increase of $\dot{\alpha}$ on stall delay is well known (references 38 and 39).

As regard the effect of $\bar{\alpha}$ on the stability, it is more difficult to identify. Indeed, amplitude should be associated with the mean angle of attack, the unsteady phenomena varying in a different manner according to the position of the steady flow stall angle relative to the range of angle of attack analysed.

7. ANALYSIS OF LOCAL AERODYNAMIC PHENOMENA ON OSCILLATING AIRFOILS

7.1. LOCAL MEASUREMENTS : PHYSICAL FACTS AND SEMANTIC PROBLEMS

The pressure measuring method offers the great advantage of giving the chordivise pressure distribution, even if it does not allow reaching the C_D in unsteady conditions, this pressure distribution being a basic data in the understanding of phenomena.

Figure 14 shows, as an example, the differential pressure variation, measured by the 13 transducers, during a cycle for two different oscillation frequencies. It is to be noted that sometimes there is a lack of accuracy in the measurement of absolute pressures.

Hot films give an excellent qualitative indication of the boundary layer condition. There is no ambiguity in the determination of transition phenomena. As regard separation, the distinction, significant in unsteady conditions, between reverse flow and separation should be kept in mind (Ref. 40). This question, well discussed from the theoretical aspect (Ref. 41), raises great problems for an experimental approach. The simple hot films, which were at our disposal, were not sufficient to describle accurately the phenomena. It would have been necessary to have, in addition, directional hot-wire probes to determine reverse flows, as this has been done in the noteworthy experiments described in reference 42.

As the distinction between reverse flows and flow separation areas of high turbulence could not be established, we have identified all these phenomena by the general term «B.F» (Beginning fluctuations). The angles of attack α_{BF} can be with the previous reserves, assimilated roughly to the angles of attack causing local separation of the boundary layer.

7.2. DYNAMIC STALL ON OSCILLATING AIRFOILS

Many papers dealing with this subject. We shall retain only the excellent synthesis given in references 39 and 43. The actual variation in differential pressures during a cycle is shown on figure 15. The mean oscillation angle of attack ($\alpha_m = 15^o$) is, in this case, close to the steady stall angle of attack ($\alpha_{ss} = 15.4^o$) of the BV 23010 – 1.58 airfoil.

In these phenomena, the process is as follow :

- When the angle of attack increases, the development of a succion area on the leading edge upper surface contributes, as in steady conditions, to the lift increase.
- When the angle of attack exceeds the steady stall point, lift still continues to increase. This is due to the existence, in the leading edge vicinity, of an organized Vortex system which can be shown by hydrodynamic visualisation (Ref. 44).

Furthermore, the Vortex system presence leads to an increase in slope ($d\, C_N/\partial\alpha$).

- The BV 23010-1.58 airfoil having a trailing edge stall in the present experimental conditions, the alteration of aerodynamic conditions in this airfoil area, leads to a moment stall ($\alpha = 18.3^o$) immediately followed by the vortex motion towards the trailing edge. This increases the value of the nose-down moments.
- The vortex motion results in the loss of the negative pressure area, the lift stall being achieved only when the vortex has moved some distance towards the trailing edge ($\alpha = 21.3^o$).
- When the angle of attack decreases, the flow is fully separated. The loss of the main vortex leads to a reduction in the amplitude of the negative moment. A secondary vortex appears at the leading edge (between $\alpha = 18.8^o$ and 13.1^o). This results in a slight lift increase but, particularly, in a secondary loop in the moment cycle, which positively contributes to damping.
- At last, flow separation ceases at angles of attack smaller than that of steady stall.

On Figure 16, relative to the same experimental conditions, it is possible to precise this variation by associating the upper surface absolute pressure measurements to the variation in global aerodynamic coefficients. The trailing edge type stall is proved by the fact that the moment stall occurs before the fluctuations (characterizing the turbulence associated with reverse flow and/or separation) reach the x/c = 0.12 station. Lift continues to increase until the vortex, having moved away from the leading edge, reaches the x/c = 0.12 station. The loss of succion, following this motion, results in a lift decrease, while the vortex moving towards the rear of the airfoil causes a rearward motion of the aerodynamic centre and the development of large nose-down moments. The vortex velocity, estimated from the motion of the overspeed peak, has been found to be equal to 0.2 V_∞.

By using hot films, it has been possible to show that when the above phenomena occur, the boundary layers were turbulent over the greatest part of the airfoil. In fact, transition is occurring rapidly when the angle of attack increases, although the unsteady effects, reflected by the reduced frequency increase, induce hysteresis phenomena, clearly visible on figure 17.

When the angle of attack increases, the laminar-to-turbulent flow transition occurs at an angle of attack greater than that corresponding to steady conditons. Conversely, on decreasing angle of attack, the passage from turbulent to laminar flow occurs at a smaller angle of attack.

This hysteresis phenomena, showing up at M = 0.2, is noted again at M = 0.3, but at a lower global angle of attack level, due to the increase in local velocities resulting from the increase in upstream Mach number.

There hysteresis phenomena may be evaluated by a calculation of the unsteady boundary layers (Ref. 45).

The unsteady stall process, and sometimes, its kind strongly depend on motion parameters : amplitude, reduced frequency, mean angle of attack, as it may be seen on figures 18 to 20. Although the stall delay is, as it is well known, an increasing function of angular velocity $\dot{\alpha} > 0$, and reduced frequency is presented as the main parameter, it is not useless to emphasize the fact that dynamic stall strongly depends on the way the rate of change is achieved. On figure 18, the amplitude influence is shown for an oscillation at constant reduced frequency about the static stall angle of attack for the BV 2310 – 1.58 airfoil.

The amplitude seems to have a pronounced effect on the vortex system intensity and on the moment in the cycle when it leaves the leading edge to move over the upper surface.

At low frequency ($\bar{\alpha} = \pm 3^o$), vortex is very diffuse and seems to leave the leading edge at the top of cycle. Although the negative pressures are at a general higher level than in steady conditions (this explaining the C_N max. increase), stall is similar to a quasi-static stall as it is shown by the pressure curve at x/c = 0.12 of figure 18.

At the highest amplitude ($\bar{\alpha} = \pm 6^o$), vortex is more intense but it leaves the leading edge sooner in the cycle (but at an angle of attack greater than $\alpha = 18^o$). Stall has a more pronounced dynamic character. The mechanism is the same for the SA 13109 – 1.58 airfoil and explains the results shown on figure 13 where the vortex intensity at $\bar{\alpha} = \pm 6^o$, induces, at the same maximum angle of attack, very high values of C_N max. but, introduces also, by moving over the upper surface, very strong nose-down maximum moments.

Figure 19 shows the strong effect of frequency on the various stall processes. At the lowest reduced frequency (k = 0.02), we find again a generalized stall having a quasi-static characteristic, with a boundary layer separation at x/c = 0.12, occurring soon after the static stall angle of attack.

When the reduced frequency increases, there is a general out-of-phase condition in the «moment stall/ separation at x/c = 0.12/ lift stall» sequence, all these phenomena occurring on increasing angle of attack at k = 0.13 and on decreasing angle of attack at k = 0.26.

This out-of-phase condition explains the beneficial effect of reduced frequency on C_N max. and on the angle of attack at the beginning of instability. The C_N max. level, reached in stall conditions, depends on the possible formation of secondary vortices on the leading edge, the stall in decreasing angle of attack conditions having also a prejudicial effect on stability.

Figure 20 shows, at iso-amplitude, the combined effect of frequency and mean angle of attack on trailing edge stall for the OA 209 airfoil, at oscillations close to or greater than the static stall angle of attack ($\alpha_{ss} = 12.8^o$).

The hot films characterize the separation up-motion from the trailing edge towards the leading edge, while overspeeds indicate the Vortex passage. It is noted that the frequency increase, at a given α_m, delays the separation motion and Vortex appearance. The increase in mean angle of attach offsets the whole sequence which, then, occurs sooner in the cycle. All the stalls corresponding to these experimental cases occur on increasing angle of attack, except the lift stall at $\alpha_m = 12^o$ and k = 0.146.

8. DYNAMIC STALL AND PREDICTION METHODS

As nobody can calculate accurately the static stall, it is obvious that the problem is stil more insoluble for dynamic conditions. A judicious approach to the problem, particularly if it should maintain a practical character for the designer, cannot be, therefore, entirely theoretical (Ref. 46).

- We will mention only, as reference, the digital resolution methods for the complete Navier Stokes equations.
  In fact, although these methods exceed the natural limitations of the potential and boundary layer theories (Ref. 47), they are very cumbersome from the programmation aspect and applicable to very low Reynolds numbers only.

- The «unsteacy potential methods» should allow by associating simplicity and relative accuracy, the calculation of unsteady flows occurring before the dynamic stall. Figure 21 shows the results obtained, in compressibility conditions, using a model developed by Mc Croskey (ref. 48). The contributions due to the camber and airfoil thickness effects are calculated using «steady» methods. The unsteady effects are related to the angle of attack only, and calculated using the oscillating flat plate solution (Theodorsen's function for the linear formula). A non-linear formula of this model greatly improves the accuracy of results, for an angle of attack close to the static stall angle. The improvement is spectacular in the leading edge area. This formula consists in retaining terms of the second order in the Bernoulli's General equation.

  The wake action is expressed no longer in the form of an explicit function of the reduced frequency (Theodorsen's function) but using digital integrals expressing the reduced frequency and the chordwise position of the point considered on the airfoil.

  Beside its prediction accuracy of the pressure distribution, it has been possible with this model to impute part of the stall delay beyond the static stall to the effects of the unsteady perfect fluid. This idea, developed by Carta (ref. 49) for a flat plate and checked by Mc Croskey (ref. 48) for a symmetric airfoil, may be extended to a cambered airfoil, as shown on figure 22. It may be seen that, with respect to steady conditions, the unsteady effects reduce the pressure gradients over the whole airfoil. Therefore, this may explain partially the stall delay.

- The «discrete potential vortex» methods give additional information as they take into account a leading edge vortex system.
  These methods are full of promises (ref. 50). However, they are cumbersome, and often it is necessary to call on experimental data to determine the moment of vortex appearance.

- The boundary layer methods
  If they do not allow the direct calculation of dynamic stall, they give, however, additional information on stall delay. Mc Croskey has shown (ref. 45 and 46) that, due to the pressure gradients at high angle of attack, the unsteady effects are negligible near the leading edge but significant for the calculation of boundary layers on the airfoil rear section. From this it results that the laminar «loci of vanishing wall shear» varies very little in laminar flow conditions (leading edge area), but has a strong hysteresis in turbulent at the rear of airfoil. This explains also partially the stall delay.

  For additional information, it is necessary to consider a coupling between the inviscid and viscous flows in the separation area (Ref. 51).

- Synthetisation methods
  Their purpose is to correlate, in the most simple manner, the experimental results to «extend» the potential calculations in the stall conditions. Figure 23 shows, for airfoils, having trailing edge dynamic stall characteristics, a simple synthetisation, calling on angular velocity and acceleration, to express the local boundary layer separation. Linear laws have been established for other Mach numbers and by applying them it is possible to follow the separation point motion towards the leading edge versus the airfoil movement.

  Studies are in progress to determine the correlation between the moment of vortex start and the separation point motion law.

  Figure 24 shows the appreciable effect of the introduction of unsteady stall in a linear calculation method of rotor loads (ref. 24). The method used here, calls on parameter ($\dot{\alpha}$) only. Obviously, results would be still further improved if the parameter ($\ddot{\alpha}$) was also considered.

9. CONCLUSIONS

Through the experiments conducted on models oscillating about the pitch axis, it is possible to describe partially the unsteady effects on a rotor. The set-up, made by C.E.A.T, has allowed the solution of the methodological problems raised by this kind of experiment.

The research work made has allowed the determination of unsteady characteristics for many airfoils and the explanation of the trailing edge stall unsteady process.

The prediction models developed are based on simple perfect fluid models and synthetisation of experimental results. Through them, it has been possible to demonstrate the relative influence of the perfect fluid and boundary layers on stall delay. The synthetisation of boundary layer separation results seems to be an element full of promise in the establishment of a practical model of trailing edge stall delay for the airfoils presently used by Aerospatiale.

ACKNOWLEDGEMENTS

The present study is part of a research programme on «unsteady flow aerodynamics» conducted jointly by Aerospatiale, CEAT, IMFM and ONERA.

The writers are indebted to all the engineers having participated in this programme and, particularly, J.J. Philippe, ONERA engineer. They offer their thanks to W.J. Mc Croskey and to the «AMES Research Center» Aerodynamics Group, whose work has been a very precious guide and with whom they have had fruitful exchanges of views.

SYMBOLS

b : airfoil semi-chord, m

c : airfoil chord, m

$C'(k) = F + i\,G$, Theodorsen function

C_M : quarter-chord pitching moment coefficient

$C_{M\,max}$: maximum negative pitching moment coefficient

C_N : normal - force coefficient

$C_{N\,max}$: maximum positive normal-force coefficient

C_P : instantaneous pressure coefficient

$\Delta C_P = C_{P\,lower} - C_{P\,upper}$, instantaneous differential pressure coefficient

f : frequency of airfoil oscillation, Hz

$k = \frac{\pi f c}{U\infty}$, reduced frequency

M Mach number

p static pressure

p_T total pressure

$R_e = \frac{U\infty c}{\nu}$, Reynolds number

$S^* = \frac{\oint C_M\, d\alpha}{-\frac{\pi}{2}^2\, \bar{\alpha}^2 k}$ Damping ratio

t : time

$U\infty$: free - stream velocity, m/s

V : local velocity, m/s

$V^* = \frac{V}{U\infty}$ reduced local velocity

x : chordwise coordinate measured from the leading edge, m

$X : \frac{x}{c}$

α : angle of attack

α_m : mean angle of attack

$\bar{\alpha}$: oscillatory amplitude

$\dot{\alpha}$, $\ddot{\alpha}$: angular speed and acceleration

β : Flapping angle

θ : Torsional angle

ψ : Blade azimuthal position

$\omega = 2\pi f$ oscillatory frequency rd/s

Ω : rotor rotational frequency

ℓ : density kg/m^3

SUBSCRIPTS

u : upper surface

ℓ : lower surface

∞ : free stream

DS : dynamic stall

SS : static stall

REFERENCES

1) G. PETIT, Grandes tendances actuelles de l'hélicoptère, l'Aeronautique et l'Astronautique no 48, 1975-5.

2) R.A. ORMISTON, Comparaison of several methods for predicting loads on hypothetical helicopter rotor, NASA SP-352, Rotorcraft Dynamics, 1974, paper no 56.

3) P.F. YAGGY, I.C. STATLER, Progress in rotor-blade aerodynamics, AGARD Conference Proceedings no 121, Advanced rotorcraft, Sept. 1971.

4) F.J. Mc HUGH, F.D. HARRIS, «Have we overlookeed the full potential of the conventional rotor ?», 31st Annual National Forum of the A.H.S. (1975).

5) F.D. HARRIS, F.J. TARZANIN, R.K. FISHER, Rotor high speed performance, theory vs. test, J.A.H.S. vol 15 no 3 (1970).

6) C.E.K. MORRIS, Rotor-Airfoil Flight investigation : Preliminary results, 34th Annual National Forum of the American Helicopter Society (1978).

7) F.J. DAVENPORT, J.V. FRONT, Airfoils sections for rotor blades. A reconsideration, A.H.S. 22th Annual National Forum Washington (1966).

8) J. SHEIMAN, H.L. KELLEY, Comparison of flight measured helicopter rotor blade chordwise pressure distributions with static two-dimensional airfoil caracteristics, NASA TND 3936.

9) N.D. HAM M.I. YOUNG, Torsional oscillation of helicopter blades dues to stall, Journal of aircraft vol. 2 no 3 (1966).

10) F.O. CARTA P.J. ARCIDICONO H.L. ELMAN, Analytical study of helicopter rotor stall flutter, A.H.S. 26th Annual Forum Washington (1970).

11) F.O. CARTA G.L. COMMERFORD R.G. CARLSON, R.H. BLACKWELL, Investigation of airfoil dynamic stall and its influence on helicopter control loads, U.S.A.A M.R.D.L. T.R. 72-51 (1972).

12) F.O. CARTA G.L. COMMERFORD R.G. CARLSON, Determination of airfoil and rotor blade dynamic stall response, J.A.H.S. vol 18 no 12 (1973).

13) T.S. BEDDOES, Retreating blade stall flutter, westland R.P. 531 (Nov 1976).

14) M. KRETZ, Research in multicyclic and active control of rotary wings, first European Rotorcraft and Powered lift Aircraft Forum, Southampton (Sept 1975).

15) R. DAT, Aeroelasticity of rotary-wing aircraft, AGARD Lecture serie no 63 on helicopter aerodynamics and dynamics.

16) C.T. TRAN J. RENAUD, Theoretical predictions of aerodynamic and dynamic phenomena on helicpter rotors in forward flight, First European Rotorcraft and Powered lift aircraft Forum, Southampton 1975.

17) J. RENAUD F. NIBELLE, Effects of the airfoil choice on rotor aerodynamic behaviour in forward flight, Second European Rotorcraft and Powered Lift Aircraft Forum, Bückeburg 1976.

18) H. GLAUERT, on the vertical ascent of a helicopter, Aeronautical Research council no 1132 (1927).

19) N. MILLER J.C. TANG A.A. PERLMUTTER, theoretical and experimental investigation of the instantaneous induced velocity field in the wake of a lifting rotor, U.S.A.A.V.L.A.B.S. J.R. 67-68 (1968).

20) J.J. COSTES, Unsteady aerodynamics of helicopter rotors, AGARD Report no 595 (1972).

21) A.J. LANDGREBE M.C. CHENEY, Rotor wakes key to performance prediction, AGARD Conference Proceedings no 111

22) J.D. KOCUZEK TANGLER, A prescribed wake lifting surface hover performance Analysis, 32nd Annual Forum of the American Helicopter Society, May 1976.

23) F.X. CARADONNA M.M. ISOM, Numerical calculation of unsteady transonic potential flow over helicopter rotor blades, A.I.A.A. Journal vol 14 no 4, Apr. 1976.

24) J.J. COSTES, Introduction du décollement instationnaire dans la théorie du potentiel d'accélération, application à l'hélicoptère, La Recherche Aérospatiale, no 3 1975.

25) J. COUSTEIX, Progrès dans les méthodes de calcul des couches limites turbulentes bi et tridimensionnelles, ONERA N.T. 1976-15.

26) J.J. THIBERT, J. GALLOT, A new airfoil family for rotor blades, 3rd European Rotorcraft and Powered Lift Forum, Aix-en-Provence, 1977.

27) L. DADONE, Rotor Airfoil optimization : an understanding of the physical limits, 34th Annual National Forum of the American Helicopter Society, 1978.

28) J. LIIVA et al. , Two-dimensional tests of Airfoils oscillating near stall, U.S.A.A.V.L.A.B.S TR 68-13, 1968.

29) L. GRAY et al. , Wind-tunnel tests of thin airfoils oscillating near stall, U.S.A.A.V.L.A.B.S TR 68-89, 1969.

30) R.I. WINDSOR, Measurement of aerodynamic forces on an oscillating airfoil, U.S.A.A.V.L.A.B.S TR 69-98

31) J. VALENSI J. REBONT J. RENAUD G. VINGUT, Effets aerodynamiques sur un profil d'aile animé d'un mouvement harmonique parallèle à l'écoulement, AGARD CP no 11, 1973.

32) J. REBONT, C. MARESCA, D. FAVIER, J. VALENSI Dynamic reattachment on an aerofoil performing oscillations parallel to the undisturbed stream, FDP AGARD Meeting, Ottawa 1977.

33) T.S. BEDDOES, A synthesis of unsteady aerodynamic effects including stall hysterisis, First European Rotorcraft and Powered Lift Aircraft Forum.

34) Th. THEODORSEN, General theory of aerodynamic instability and the mecanism of flutter, NACA 496, 1940.

35) J. COULOMB, Moyen d'essais pour l'étude d'écoulements instationnaires autour de profils en oscillation d'incidence, 14ème colloque d'Aérodynamique Appliquée, Toulouse 1977.

36) W.J. Mc CROSKEY E.J. DURBIN, Flow angle and shear stress measurements using heated films and wires, Traésactions of the AS ME vol 94 no 1, March 1972.

37) J.J. PHILIPPE, Le décrochage dynamique : un exemple d'interation forte entre écoulements visqueux et non visqueux, réunion AGARD sur l'Aerodynamique Instationnaire, Ottawa Sept. 1977.

38) D. GROSS F.D. HARRIS, Prediction of inflight stalled airloads from oscillating airfoil data, 25th Annual National Forum - AHS - 1969.

39) W.J. Mc CROSKEY, Recent developments in dynamic stall, symposium on unsteady aerodynamics, TUCSON 1975.

40) W.R. SEARS D.P. TELIONIS, Unsteady boundary layer separation, IUTAM Symposium on unsteady boundary layers, QUEBEC 1971.

41) Symposium on unsteady aerodynamics, TUCSON 1975.

42) L.W. CARR K.W. Mc ALISTER W.J. Mc CROSKEY Analysis of the development of dynamic stall based on oscillating airfoil experiments, NASA TN D-8382, 1977.

43) W.J. Mc CROSKEY, Some current Research in unsteady Fluid dynamics, the 1976 Freeman Scholar Lecture.

44) H. WERLE, Visualisation hydrodynamique d'écoulements instationnaires, IUTAM Symposium on recent research in unsteady boundary layers, QUEBEC 1972.

45) W.J. Mc CROSKEY J.J. PHILIPPE, unsteady viscous flow on oscillating airfoils, AIAA 12th Aerospace Sciences Meeting, Washington 1974.

46) W.J. Mc CROSKEY, Prediction of unsteady separated flows on oscillating airfoils, AGARD Lecture Series no 94 on three dimensional and unsteady separation at high Reynolds numbers.

47) U.B. MEHTA, Dynamic stall on an oscillating airfoil, AGARD CP-227, 1977.

48) W.J. Mc CROSKEY, Inviscid flowfield on an unsteady airfoil AIAA 5th Fluid and Plasma Dynamics Conference, Boston 1972.

49) F.O. CARTA, A theoretical study of the effect of unsteady pressure gradient on dynamic stall delay, Journal of Aircraft 10, 1971.

50) N. BAUDU M. SAGNER, Modélisation du décrochage dynamique d'un profil oscillant, 10ème Colloque AAAF d'Aerodynamique appliquée, Lille 1973.

51) P. CRIMI B.L. REEVES, A method for analyzing dynamic stall on helicopter rotor blades, NASA CR-2009, 1972.

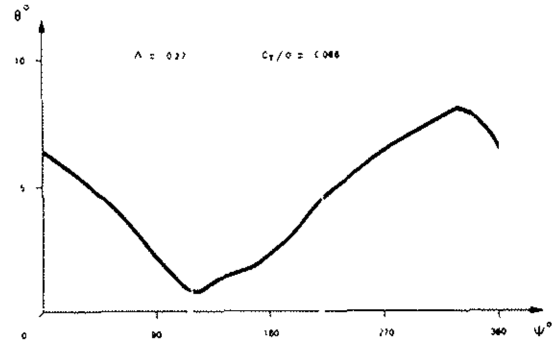

FIGURE 1 : TYPICAL TORSIONAL BLADE MOTION

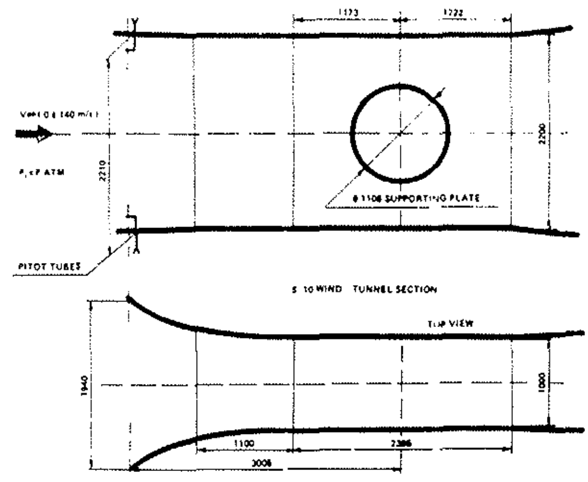

FIGURE 3 : TEST SECTION CHARACTERISTICS

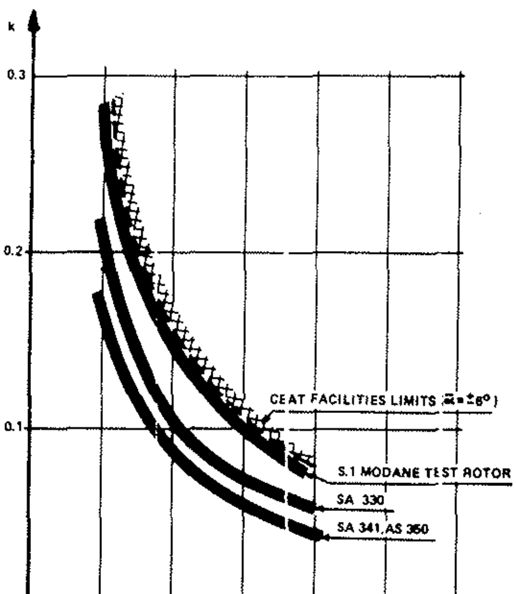

FIGURE 2 : CEAT RIG REDUCED FREQUENCY SIMULATION MAIN ROTOR (1 Ω)

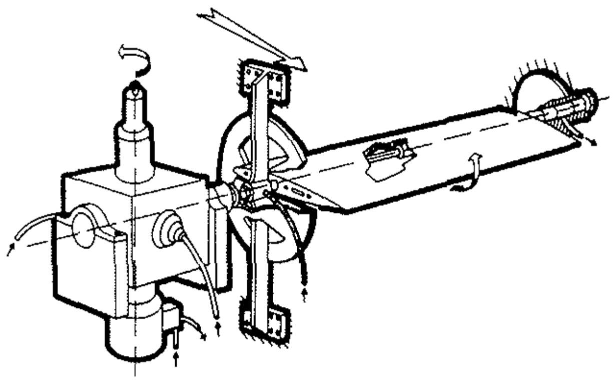

FIGURE 4 : PITCH OSCILLATING MECHANISM (S. 10 TOULOUSE)

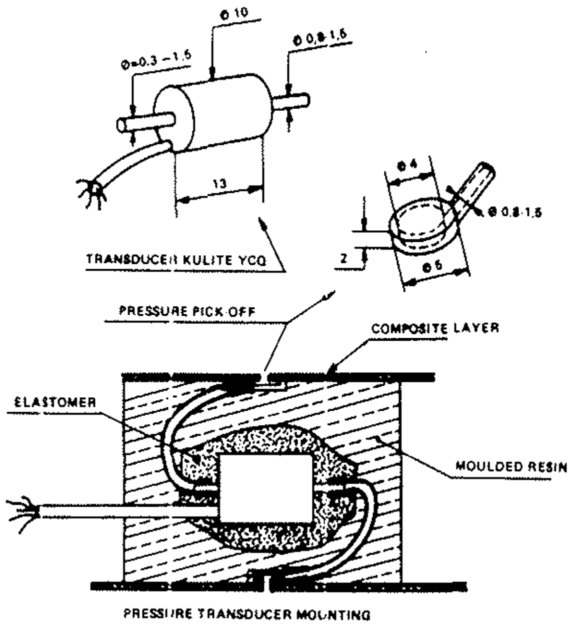

FIGURE 5 : PRESSURE TRANSDUCER MOUNTING

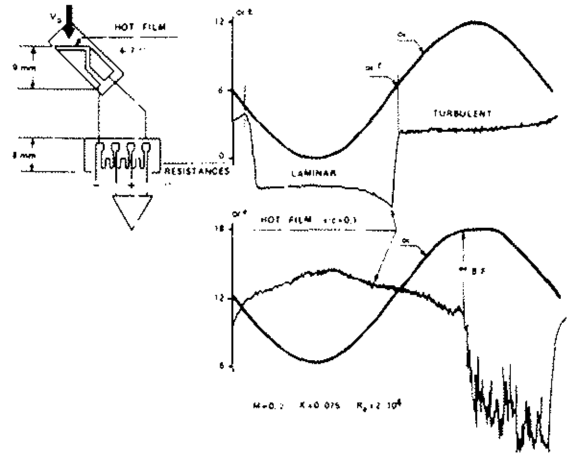

FIGURE 7 : HOT-FILM INSTALLATION AND TYPICAL DATA RECORDING

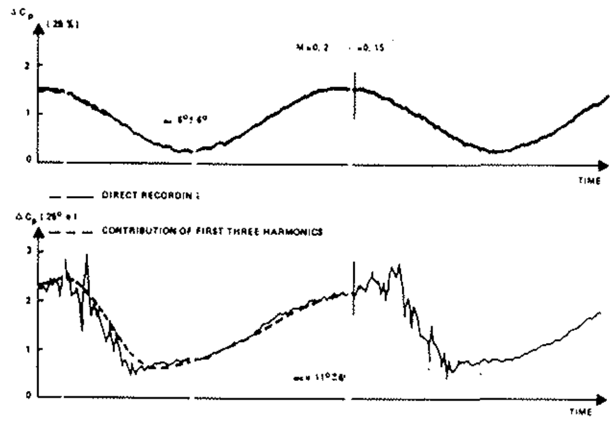

FIGURE 6 TYPICAL PRESSURE TRACE AND DATA REDUCTION

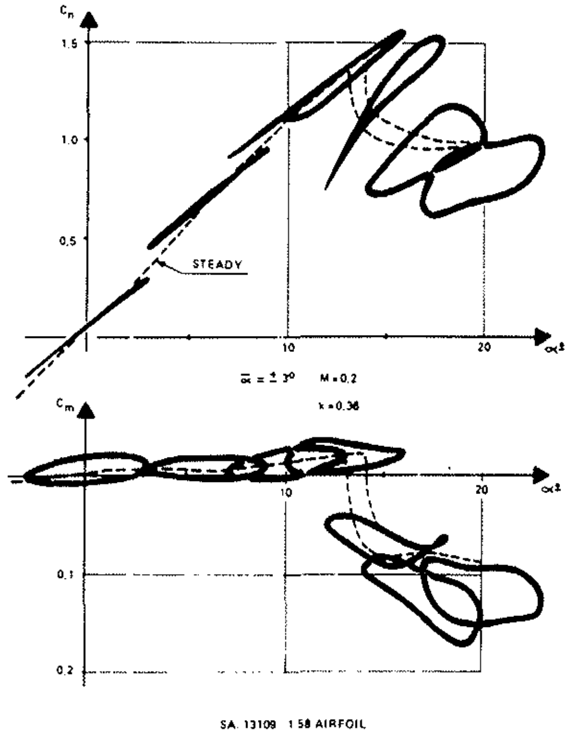

FIGURE 8 : DYNAMIC LIFT AND MOMENT COEFFICIENTS VERSUS ANGLE OF ATTACK

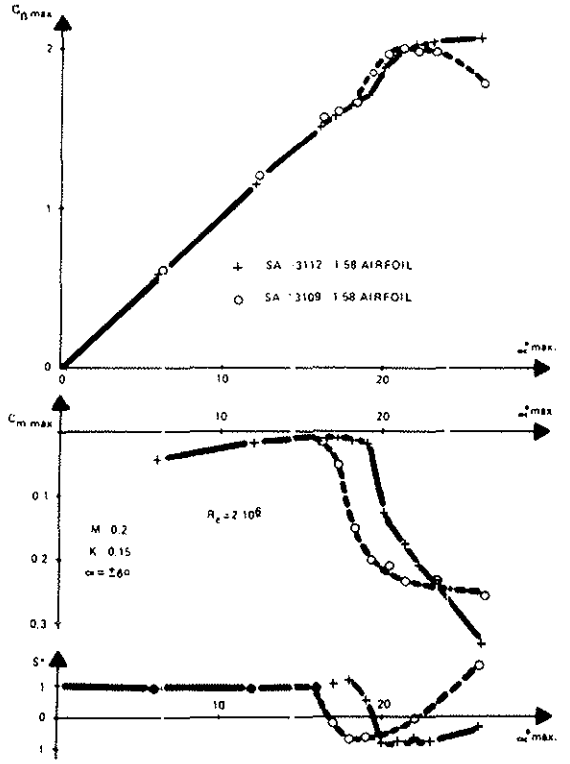

FIGURE 9 : INFLUENCE OF AIRFOIL THICKNESS ON DYNAMIC CHARACTERISTICS

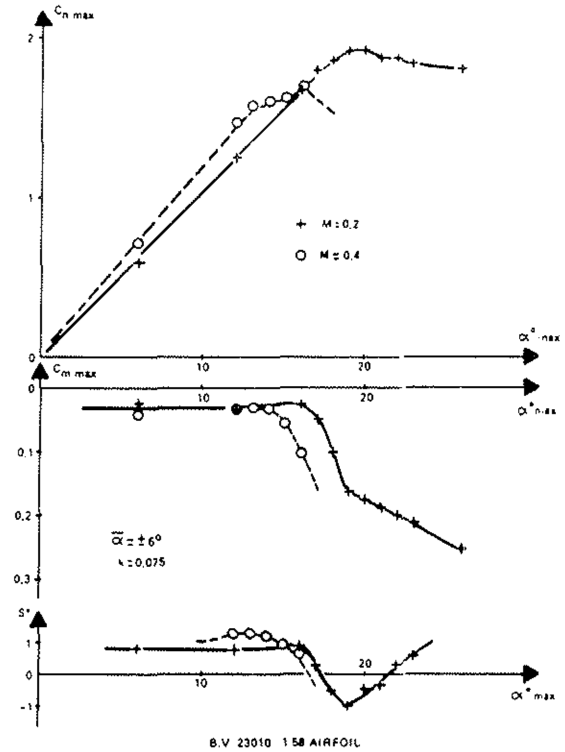

FIGURE 11 : MACH NUMBER EFFECT ON AIRFOIL DYNAMIC CHARACTERISTICS

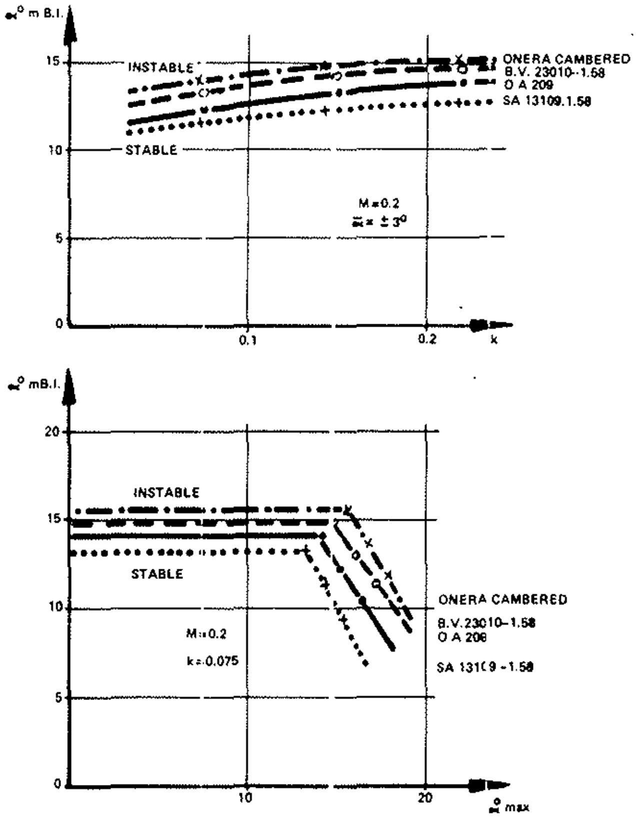

FIGURE 10 : INFLUENCE OF AIRFOIL GEOMETRY ON THE LOWER INSTABILITY LIMIT

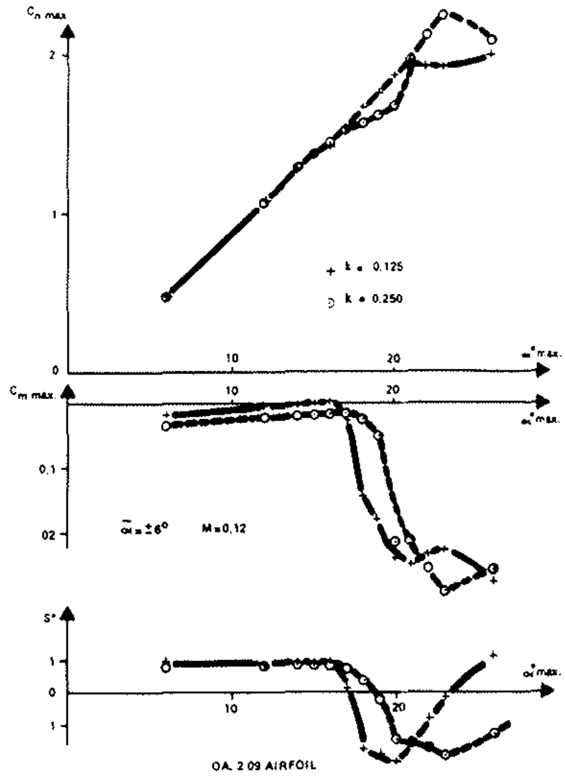

FIGURE 12 : EFFECT OF FREQUENCY ON AIRFOIL DYNAMIC CHARACTERISTICS

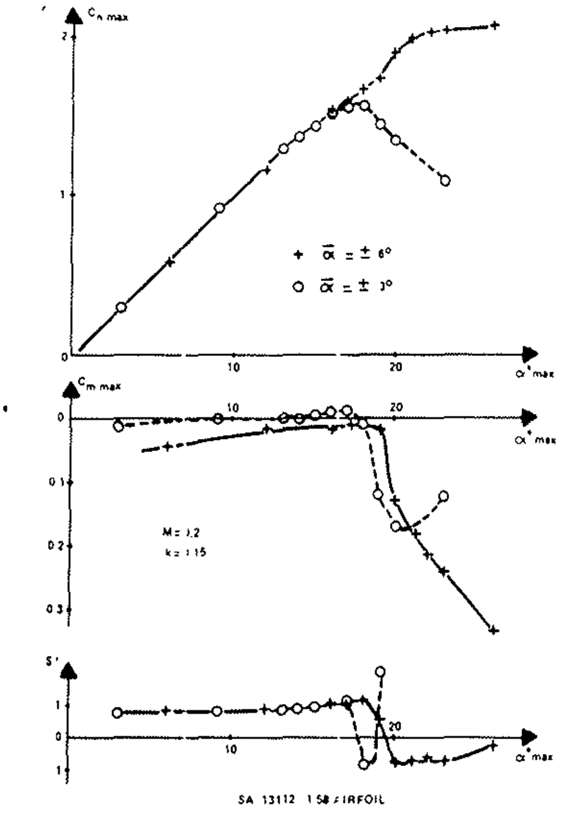

FIGURE 13 : AMPLITUDE EFFECT ON AIRFOIL DYNAMIC CHARACTERISTICS

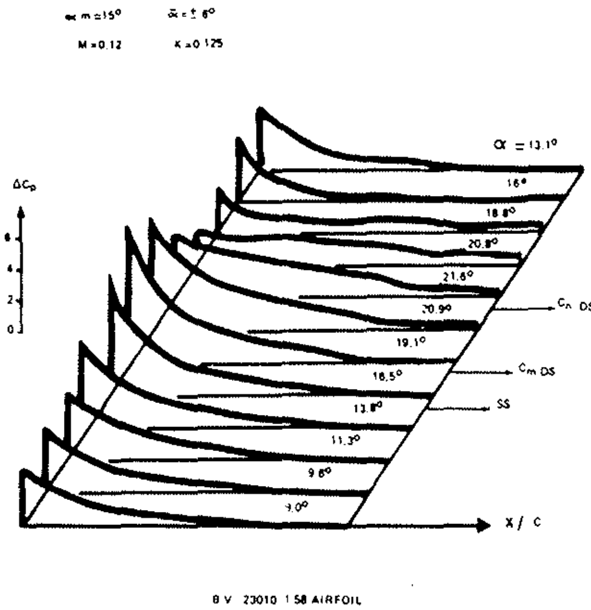

FIGURE 15 : TIME - HISTORY OF DIFFERENTIAL PRESSURE DISTRIBUTION DURING A CYCLE ABOUT STATIC STALL ANGLE

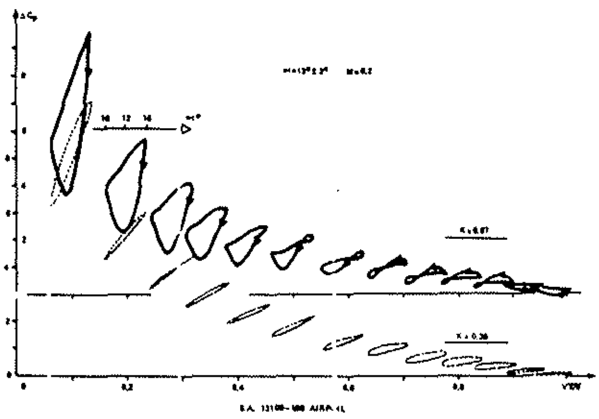

FIGURE 14 : VARIATION OF DIFFERENTIAL PRESSURES DURING A CYCLE 13 CHORDWISE POSITIONS

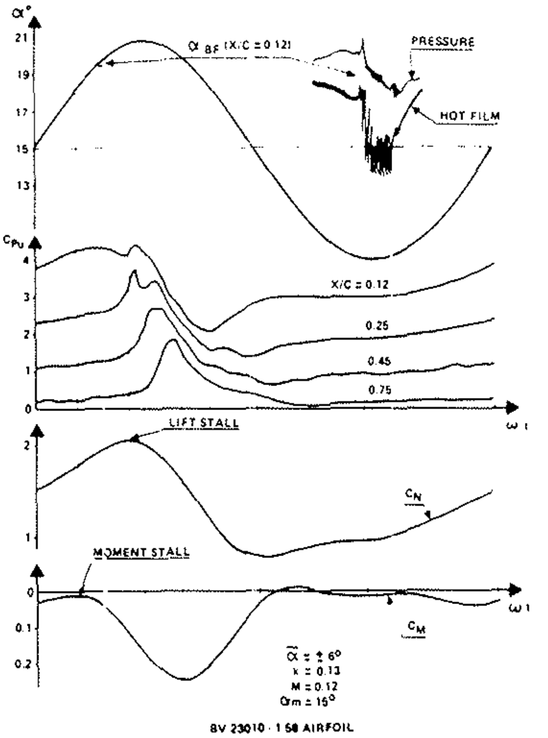

FIGURE 16 : TIME - HISTORY OF LOCAL AND GLOBAL AERODYNAMIC PARAMETERS DURING A CYCLE

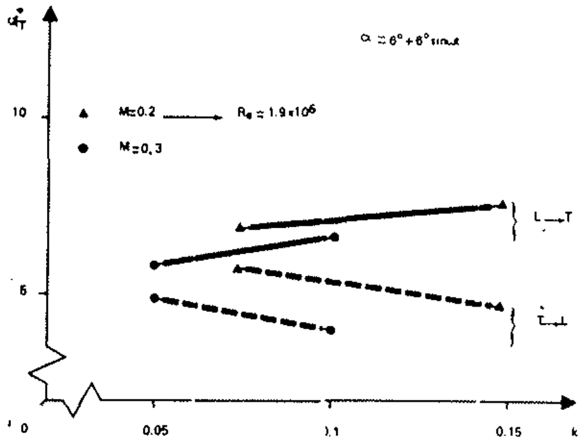

FIGURE 17 : EFFECT OF REDUCED FREQUENCY ON TRANSITION OA 209 AIRFOIL UPPER SURFACE X/C = 0.12

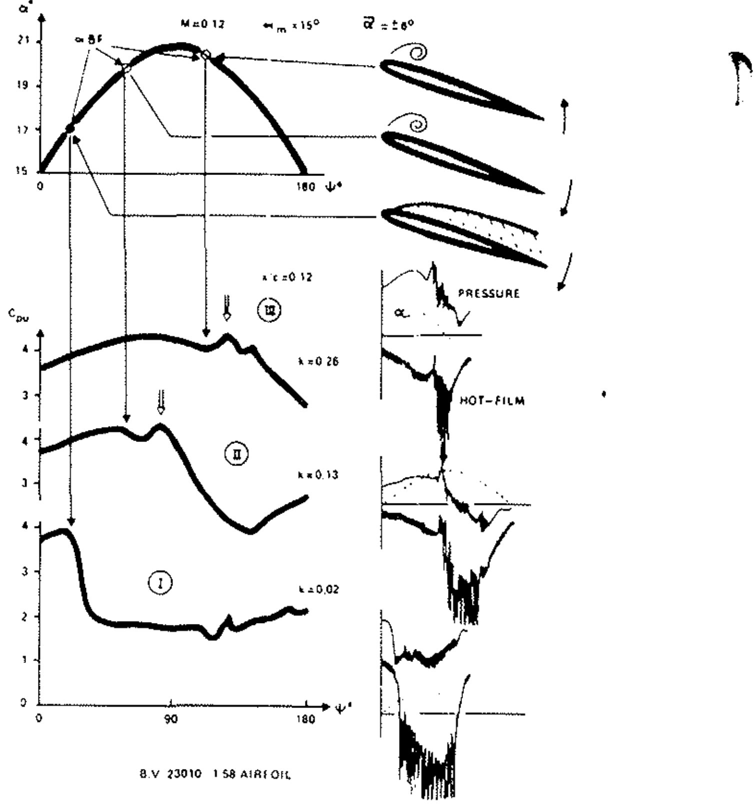

FIGURE 19 : INFLUENCE OF FREQUENCY ON STALL

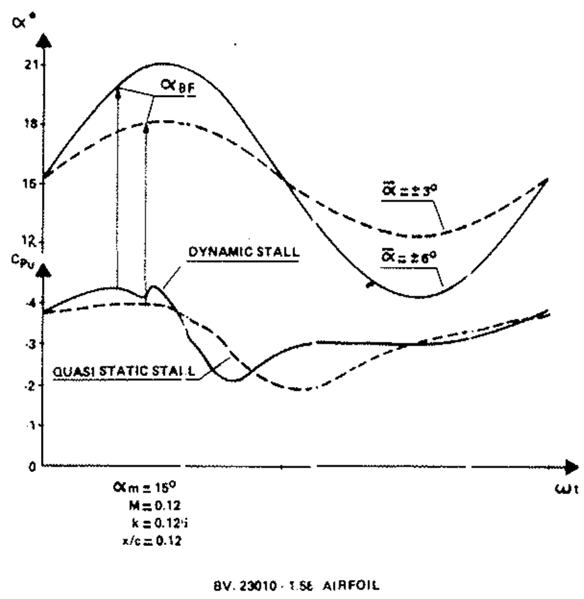

FIGURE 18 : AMPLITUDE EFFECT ON STALL

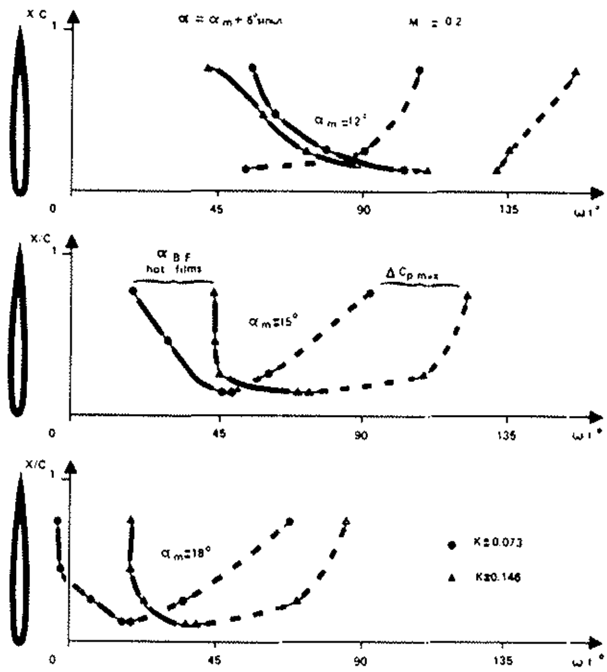

FIGURE 20 : DYNAMIC STALL PROCESS ON THE OA209 AIRFOIL

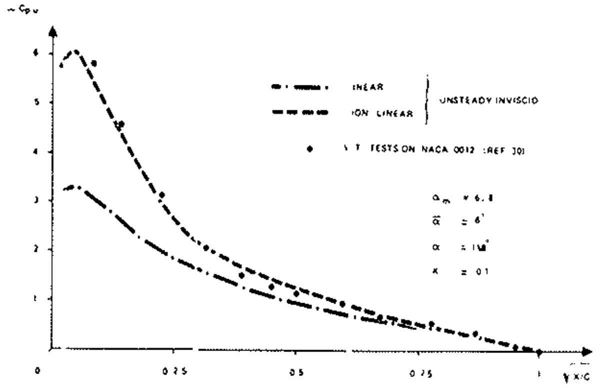

FIGURE 21 : EFFECT OF NON - LINEARITIES (INVISCID FLUID) ON UPPER SURFACE PRESSURES

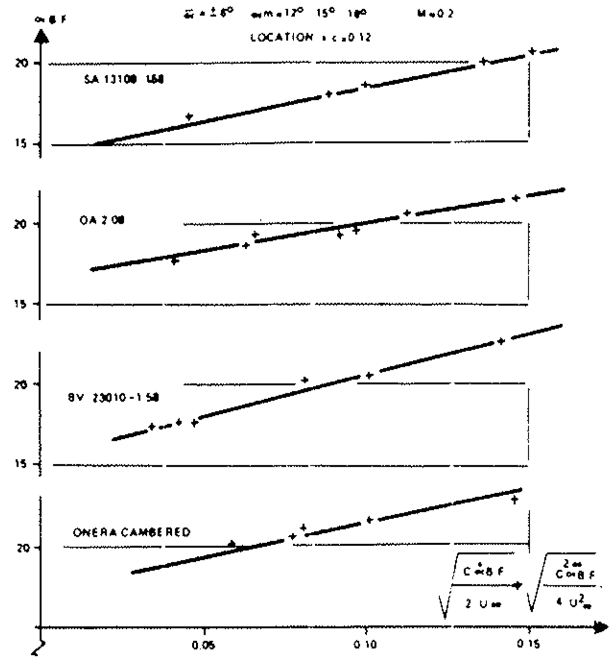

FIGURE 23 : SYNTHETIZATION OF DYNAMIC SEPARATION OCCURENCE

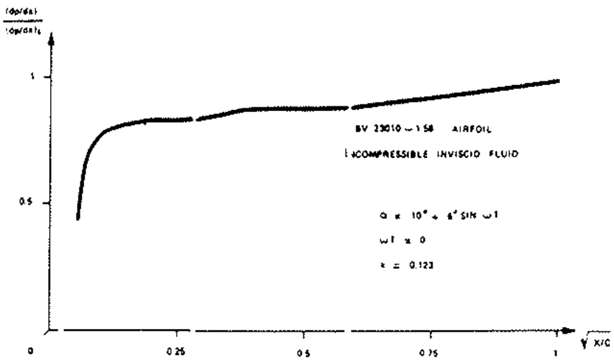

FIGURE 22 : UNSTEADY EFFECT ON PRESSURE GRADIENT

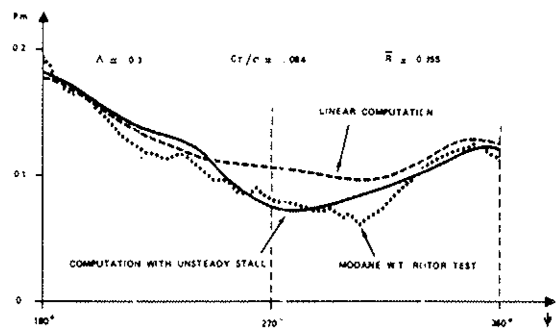

FIGURE 24 : EFFECT OF DYNAMIC STALL ON CALCULATED ROTOR LOADS